ISSN 1068-3739, Russian Meteorology and Hydrology, 2016, Vol. 41, No. 2, pp. 136–145. Allerton Press, Inc., 2016.
Original Russian Text A.M. Kuznetsova, G.A. Baidakov, V.V. Papko, A.A. Kandaurov, M.I. Vdovin, D.A. Sergeev, Yu.I. Troitskaya, 2016, published in Meteorologiya i Gidrologiya, 2016, No. 2, pp. 85–97.

Field Experiments and Numerical Modeling of Wind Speed and Surface Waves in Medium-size Inland Reservoirs

A. M. Kuznetsova[a, b], G. A. Baidakov[a, b], V. V. Papko[a, b], A. A. Kandaurov[a, b], M. I. Vdovin[a, b], D. A. Sergeev[a, b], and Yu. I. Troitskaya[a, b]

[a]*Institute of Applied Physics, Russian Academy of Sciences, GSP-120, ul. Ul'yanova 46, Nizhny Novgorod, 603950 Russia*

[b]*Lobachevskii State University of Nizhny Novgorod, pr. Gagarina 23, Nizhny Novgorod, 603950 Russia, e-mail: alexandra@hydro.appl.sci-nnov.ru*

Received November 25, 2015

Abstract—An attempt is made to apply the modern methods of surface wave simulation developed for oceanic conditions to the modeling of waves in medium-size inland reservoirs (10–100 km). The results of field measurements of wind speed and waves are described, and on their basis the parameterization $C_D(U_{10})$ is proposed. WAVEWATCH III spectral wave model was adapted to the conditions of a medium-size inland reservoir. The simulated data are compared with the field data. The use of the new parameterization $C_D(U_{10})$ allowed reducing the values of the wind wave growth rate that improved consistency in data from the field experiment and numerical modeling concerning the height of significant waves. Further steps towards improving the quality of prediction of the adapted WAVEWATCH III model are discussed.

DOI: 10.3103/S1068373916020084

Keywords: Field experiment, numerical simulation, wind-wave interaction, WAVEWATCH III

1. INTRODUCTION

The problems of surface waves, mechanisms of their generation and development, effects on the atmospheric water surface layer and impurity diffusion in the ocean, and role in the Earth climate system are the important objects of scientific interest and basic areas of research of academician G.S. Golitsyn and his followers [1]. These problems have several applications including the modeling of surface waves in the framework of spectral wave models. The present paper deals with the urgent problem of surface wave prediction in an inland reservoir using spectral wave models.

Water waves are the main reason for reservoir shore erosion. Besides, the processes of momentum, heat, and moisture exchange over the reservoir define the microclimate of adjoining territories. The accurate forecast of waves provides the safety of river navigation. To predict waves some numerical models were worked out (WAVEWATCH III [25], WAM [14], and SWAN [24]) which describe the evolution of the full two-dimensional spectrum of waves under the influence of wind-wave interaction, dissipation, and four-wave interaction. In the case of shallow water some of the models also take into account bottom friction caused by the collapse depth and three-wave interaction.

Nowadays spectral wave models are successfully used for forecasting waves on big lakes, in particular, WAVEWATCH III is used for this purpose on the Great Lakes in the USA [5, 6]. Data on the current wave conditions are presented at the open website and are updated every three hours [18]. WAVEWATCH III and SWAN models were successfully used for the hindcasting of wind and waves in the Caspian Sea and Lake Ladoga [20]. The first results of the WAM model application to wave prediction in a medium-size inland reservoir (with the linear size of 10–100 km) have recently been obtained [17]. In the present paper the WAVEWATCH III model was selected for modeling surface waves in medium-size inland reservoirs; unlike SWAN and WAM, this model allows including different parameterizations of wind-wave interaction.

The main problem of numerical simulation of waves by the WAVEWATCH III model in medium-size inland reservoirs is associated with the small fetch at which the parameters of generation and development of waves differ much from the similar parameters typical of large fetches in the open ocean [25]. Most often the numerical description of waves in medium-size lakes and reservoirs is based on numerical models [2, 4]. However, empirical relationships based on averaged characteristics cannot predict extreme conditions (for example, storm [22]) being important for solving many meteorological problems; so, the use of numerical wave models is necessary.

The features of small-fetch waves in medium-size reservoirs include more significant wind effects proportional to the ratio of wind friction velocity (or wind speed at the height of 10 m) to the wave phase velocity [25]. Another peculiarity is significant nonlinearity caused by high wave steepness. Thus, the adaption of the ocean wave model to the conditions of medium-size inland reservoirs should occur in two stages, namely, the adjustment of wind effects and the "collision integral." Dissipation caused by wave breaking is of universal nature.

One more problem of the adaptation of numerical models to the conditions of medium-size inland reservoirs is the small number of experimental data suitable for verification [7, 8]. The present paper considers the possibility of the WAVEWATCH III model adaptation to the conditions of a medium-size inland reservoir by an example of the Gorky Reservoir being a part of the Volga Cascade. The methods of field experiment in the Gorky Reservoir differ from those used in [7, 8] and are focused on studying airflow in the immediate proximity to the sea surface. The results of the numerical experiment and field experiments in the Gorky Reservoir are compared in the paper.

2. PARAMETERIZATIONS OF WIND-WAVE INTERACTION

The software system of the WAVEWATCH III model is based on the numerical solution of the Hasselman's equation for the wave action spectral density $N(k, \ ; \mathbf{x}, t)$ [25] which has the following form for the case of deep water:

$$\frac{N}{t} \quad {}_x\dot{\mathbf{x}}N \quad \frac{}{k}\dot{k}N \quad \dot{} \quad N \quad \frac{1}{}(S_{\text{nl}} \quad S_{\text{in}} \quad S_{\text{dis}}). \tag{1}$$

The left part of the equation described the wave kinematics (where $\dot{\mathbf{x}}$ is the group velocity; k is the wave number; is the angular direction). The right part includes dynamic summands: S_{nl} describes the four-wave interaction, S_{in} describes wind-induced wave growth, S_{dis} describes dissipation mainly caused by the wave collapse; is circular frequency.

In medium- and small-size reservoirs characterized by small fetches, wind effects become considerable and need more accurate description. In general case, wind effects S_{in} are specified according to the Miles model of wind-induced wave growth [21]:

$$S_{\text{in}} \quad N \ . \tag{2}$$

There is the dimensionless coefficient through which the rate of wind-induced wave height growth is expressed [21]

$$\text{Im} \quad \frac{1}{2} \quad \frac{u_*^2}{c^2} \tag{3}$$

where Im is the imaginary part of complex frequency; c is the phase velocity of the wave; the coefficient depends on wind friction velocity u_* determined through the turbulent momentum flux

$$_{\text{turb}} \quad {}_{\text{a}}\langle u_x u_z \rangle \quad {}_{\text{a}}u_*^2 \tag{4}$$

(${}_{\text{a}}$ is air density; u_x and u_z are the pulsation components of wind speed).

The experimental determination of the value of the turbulent momentum flux is a complex problem. The most widespread methods are the profiling, pulsation, and dissipation methods. In the pulsation method the momentum flux is retrieved by the direct measurement of eddy fluxes [27]. The dissipation method consists in the analysis of distribution of spectral density turbulence and is based on the assumption that there is balance between the generation and decay of turbulence. The profiling method uses the logarithmic law based on the Prandtl–Karman boundary layer theory for the flat plate: under conditions of neutral stratification the wind speed profile in the constant flow layer (where the turbulent momentum flux does not depend on height) is close to logarithmic [3]

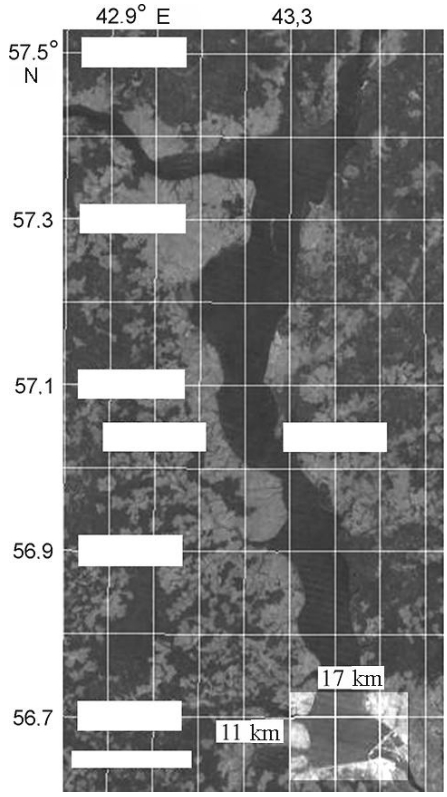

Fig. 1. The Gorky Reservoir. Data are taken from Google Earth. The light rectangle marks the measurement area.

$$U(z) \quad \frac{u_*}{} \ln \frac{z}{z_0} \tag{5}$$

where = 0.4 is the Karman constant; z_0 is the surface roughness height. By analogy with the flat plate resistance, the aerodynamic drag coefficient of water surface is introduced, it connects the measured wind speed and the turbulent momentum flux (wind friction velocity)

$$C_D \quad \frac{\text{turb}}{{}_{\text{a}}U_{10}^2} \quad \frac{u_*^2}{U_{10}^2} \tag{6}$$

where U_{10} is the wind speed reduced to the height of 10 m.

There is a number of empirical models that describe the coefficient of interaction between wind and waves . They differ much for long waves typical of the oceans but are similar in the frequency range typical of the conditions under study [29]; therefore the type of parameterization of the wind–wave interaction coefficient under conditions of medium-size inland reservoirs is not essential. Thus, to provide the more exact specification of wind effects, the parameterization of coefficient C_D is needed which defines transition from the measured speed U_{10} to the wind friction velocity u_* included into the parameterization.

Computations used the WAM 3 Snyder's parameterization [19, 23], the most convenient of the WAVEWATCH III model parameterizations from the point of view of modification. The WAM 3 model [19, 23, 28] is specified by two empirical formulae. The first formula estimates the wind-induced wave growth rate:

$$\text{Im} \quad C_{\text{in}} \frac{\text{a}}{\text{w}} \max\ 0,\ \frac{28u_*}{c} \cos(\quad {}_{\text{wind}}) \quad 1 \tag{7}$$

where $C_{\text{in}} = 0.25$ is the constant; ${}_{\text{a}}/{}_{\text{w}}$ is the ratio of air density to water density; ${}_{\text{wind}}$ is the main wind direction. The second formula represents the parameterization of aerodynamic drag coefficient of water surface C_D and was proposed in [28]

$$C_D \quad 0.001(0.8 \quad 0.65U_{10}). \tag{8}$$

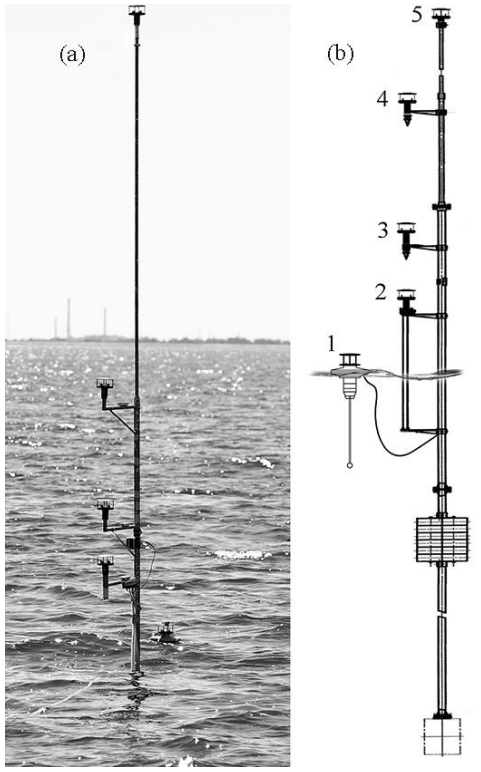

Fig. 2. (a) The photo and (b) scheme of the Froude buoy.

This parameterization provides the relation between the wind speed U_{10} and wind friction velocity $u_* \quad U_{10}\sqrt{C_D}$.

The parameterization of the dependence $C_D(U_{10})$ used to modify the WAM 3 model was proposed as a result of the series of field experiments in the Gorky Reservoir area.

3. INSTRUMENTS AND METHODS OF FIELD EXPERIMENTS

The measurements were carried out from May to October in 2012–2014 in the Gorky Reservoir area (the depth of the reservoir is 4–20 m and in the area of measurements the depth is 9–12 m). The prolate shape of the reservoir (Fig. 1) enables studying wind waves for different values of fetch depending on the wind direction.

The measuring instruments were installed at the buoy station that was originally worked out on the base of the oceanographic Froude buoy. The buoy represented a partially submerged mast that is held in the vertical position using a float near the surface and using a weight under water (Fig. 2). The total length of the buoy is 12 m and the length of its above-water part is 5.3 m. The resonance frequency of vertical fluctuations is 0.25 Hz that corresponds to the wavelength of 25 m. Four WindSonic wind speed sensors (made by Gill Instruments) were installed at the buoy mast at the height of 0.85, 1.3, 2.27, and 5.26 m (sensors 2–5). The fifth sensor (1) was located on the float tracking the wave to measure wind speed in the immediate proximity to the water surface. The distance from the float to the buoy mast was equal to about 1 m, and the height of the wind speed measurement zone from the water surface was equal to 10 cm. The buoy was equipped with the sensors of air temperature (at the height of 0.1 (a float), 0.85, and 1.3 m) and water temperature and with the three-channel string wave recorder which enables retrieving spatiotemporal profiles of waves.

WindSonic is an ultrasonic two-component wind speed sensor (the measurement error is 4% and the speed resolution is 0.01 m/s). The range of measured values of wind speed (0–60 m/s) includes the values typical of calm conditions. Resistive temperature sensors measure the temperature of the environment with the error of 3% and resolution of 0.01°C. The string wave recorder consists of three pairs of string resistive sensors located at the vertices of the equilateral triangle with the side equal to 62 mm; the sampling frequency is 100 Hz. The system allows estimating the parameters of waves whose length exceeds the double

distance between the sensors (k_{max} 0.5 cm^{-1}). The algorithm of the processing of signals received from the instrument uses the Fourier transform and is described in detail in [26] (paper [11] presents a similar algorithm using the wavelet transform).

The location of wind speed sensors corresponds to the structure of the air flow. In the presence of waves on the water surface, the stream function in the air can be represented in the form of the sum of mean and wave components [10]

$$\int_0^z U(\ )d \tag{9}$$

where z is the vertical coordinate; is the wave perturbation of the stream function. In case of a traveling monochromatic wave where the elevation of the surface z (x, t) $A\mathrm{Re}\exp(\ ik(ct\ \ x))$, can be computed from the following equation:

$$(U\ \ c)(\ \ \ k^2\ )\ \ U\ \ \ 0. \tag{10}$$

If the value of $U\ /k^2(U\ \ c)$ is much above or much below 1, the following function represents the approximate solution of the equation:

$$A(U\ \ c)\exp(\ kz) \tag{11}$$

where A is the wave amplitude. In the case of the logarithmic profile of speed (5) this condition takes the form of $u_*/\ (kz)^2\left|U\ \ c\right|$ 1 (or $u_*/\ (kz)^2\left|U\ \ c\right|$ 1) and is well met at the height z that is about the wave amplitude and higher. Thus, the basic disturbance contributed by waves to the air flux (wind bending along the surface) exponentially decreases with height. Hence, to provide the immobility of the sensor relative to the mean stream lines, the wave velocity at the distance from the water surface should be measured at the fixed level. The measurements near the surface should be carried out from the float using the sensor tracking the wave shape. It is important that the lower sensor is not located in the wave boundary layer whose value can be estimated in accordance with [9]:

$$k\ \frac{u_*}{}\ln\ \frac{z}{z_0}\ \ \ c\ \Big|_z\ \ \ \frac{u_* z}{2}\Big|_z\ . \tag{12}$$

Under conditions of the Gorky Reservoir (k = 2–3 m^{-1}, u_* = 0.1–0.4 m/s), $\sim$ 1 mm that is much below the measurement height of the lower wind speed sensor.

The study of wind flow parameters was carried out by the profiling method (see Section 2). The general record of wind speed with the duration up to 5 hours was divided into the periods of 5 minutes (300 measurement points) overlapping by 50%. As a result of the averaging, five values of wind speed corresponding to five measurement levels were obtained for each time period. The obtained mean profile was approximated by function (5) with the approximation parameters u_* and z_0. The values of wind speed U_{10} at the height of 10 m and the aerodynamic drag coefficient C_D were retrieved from the obtained approximation.

4. RESULTS OF THE FIELD EXPERIMENT

The effects of the data from separate horizons on the result of wind speed profile approximation were analyzed. Figure 3a presents the comparison of retrieved dependences $C_D(U_{10})$ for two combinations of wind speed sensors: with and without the lower sensor as well as the results presented in [7, 8] and the oceanic parameterization [12]. It is clear that the values of $C_D(U_{10})$ obtained without data from the lower sensor are higher and closer to the results presented in [7, 8, 12]. In the case of using the data from the lower sensor, the values of the aerodynamic drag coefficient are lower. Figure 3b presents the comparison of retrieved dependences $C_D(U_{10})$ using only the data of two lower sensors and the data of five sensors of wind speed. In case of using two sensors only, significant differences are observed in retrieving wind parameters in the range of small values of wind speed.

These results can be explained by the distinction of wind speed profile shape from the logarithmic one. This distinction is probably caused by the stratification of the atmospheric surface layer and by the non-stationary nature of wind because the lower part of the profile is adapted to varying wave conditions more quickly. The air flow parameters on the water–air interface define the momentum transfer from wind to waves.

Thus, the use of the lower sensor (in the case under consideration, the use of two lower sensors only) affects the measurement result considerably. To determine the correctness of the measured dependence

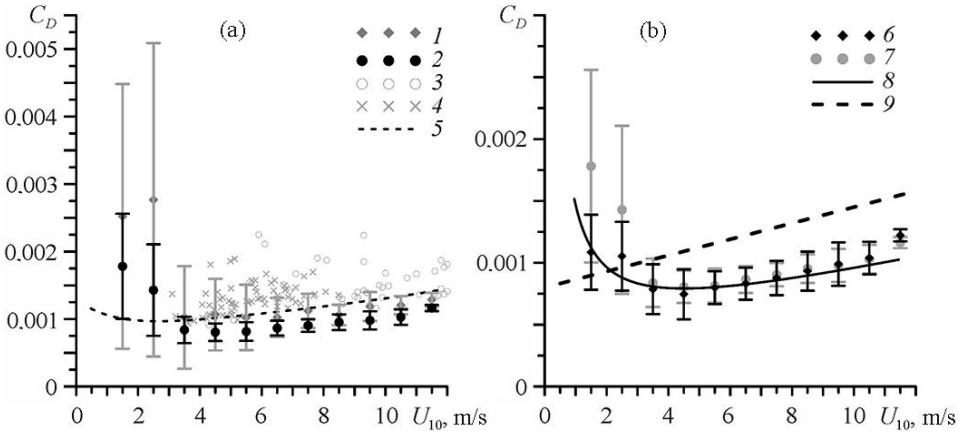

Fig. 3. The comparison of dependences $C_D(U_{10})$ retrieved using different combinations of sensors. (a) With and without the lower sensor of wind speed: (*1*) sensors 2–5 (Gorky Reservoir); (*2*) sensors 1–5 (Gorky Reservoir); (*3*) the data presented in [8] (Lake George, Australia, 2008); (*4*) the data presented in [7] (Lake Washington, USA, 1999); (*5*) COARE 3.0 parameterization; (b) the use of the whole profile of wind speed and two lower sensors: (*6*) sensors 1 and 2 (Gorky Reservoir); (*7*) sensors 1–5 (Gorky Reservoir); (*8*) approximation by function (13); (*9*) WAM 3 parameterization.

$C_D(U_{10})$, this dependence was used in the numerical modeling of wind waves in the WAVEWATCH III model. For this purpose the experimental data were approximated (Fig. 3b) by the following function:

$$C_D \quad 0.00124\,U_{10}^{1} \quad 0.00034 \quad 0.000049\,U_{10}. \tag{13}$$

5. NUMERICAL EXPERIMENT

The WAVEWATCH III model was adapted to inland reservoir conditions. For this purpose, the minimum value of significant wave height (H_s) was changed in the open software code. To describe the reservoir, the topographic grid of the Gorky Reservoir with the size of 72 108 and grid spacing of 0.00833 was used. The grid was taken from the NOAA Global Land One-kilometer Base Elevation (GLOBE) data. In view of the absence of open trustworthy bathymetric data for the Gorky Reservoir and taking into account that the navigation maps indicate the rather large depth of the reservoir, deep water approximation was chosen. Besides, the waves with the length of more than 4.5 m were not observed in field experiments. In view of this, the bottom topography was not taken into account for computations, and the depth was selected to be equal to 9 m. The frequency range was changed in accordance with that observed in the experiment, from 0.2 to 4 Hz. For the modeling it was divided into 31 frequencies and was specified by the logarithmic formula for the frequency increase $_N$ ( )$^{N\ 1}$ $_1$ where the increment = 1.1 was chosen in accordance with recommendations [25]; 31 angular directions were considered. The waves in the reservoir were simulated using the prescribed topographic data and data on the speed and direction of wind and on difference in the values of temperature at the water–air interface and at the prescribed Gaussian initial perturbation for different parameterizations of wind effects.

The range was considered of the moderate speed of wind (1–9 m/s) of different directions with the constant values over the whole Gorky Reservoir surface. In practice, reanalysis data are commonly used to specify wind effects for modeling wind waves on the sea and ocean surface. This approach is unsuitable for the water areas of medium-size inland reservoirs due to the too low spatial resolution (2.5). Besides, only two weather stations (Yur'evets and the Volga River hydrometeorological observatory) located on the shore are situated in the area under consideration. It was found that the values of wind speed in the coastal part of the reservoir and over its water area differ significantly. In view of this, computation was carried out using the input data measured in the field experiment and updated every15 minutes: the speed and direction of wind at the height of 10 m and difference in the values of temperature at the water–air interface. If the speed and direction of wind are forcedly prescribed to be the same over the reservoir, this may lead to errors in the numerical experiment because the prolate shape of the reservoir and its high shores can be a reason for considerable spatial variability with the scale of about or below 1 km.

The comparison was carried out for the following output data: one-dimensional elevation spectra, significant wave height H_s, and weighted mean wave period T_m. The value of H_s in the model and in the experiment was computed from the formula

$$H_s \quad 4\sqrt{\widehat{E}} \tag{14}$$

where $\widehat{E} \quad \int_{f_{\min}}^{f_r} E(f)df$ is full energy, $E(f)$ is the spectral density of wave force.

The weighted mean wave period T_m was computed from the following formula:

$$T_m \quad T_{m\,0,-1} \quad \int_{f_{\min}}^{f_r} E(f)df \quad \int_{f_{\min}}^{f_r} E(f) f^{\,1} df. \tag{15}$$

All model data were obtained at the point corresponding to the observational point and were averaged for 15 minutes to agree with the field experiment data averaged in a similar way.

The computations were carried out in two ways: in the framework of the WAM 3 oceanic parameterization using the linear dependence of C_D on U_{10} [28]; using the parameterization of C_D proposed by the authors and the wind-induced wave growth rate from WAM 3. Difference in parameterization is demonstrated in Fig. 3b. It is clear that if the wind speed is below 2.5 m/s, the values of C_D obtained as a result of the field experiment are higher than those obtained from the oceanic parameterization; if wind speed is above 3 m/s, the opposite picture is observed.

6. COMPARISON OF THE RESULTS OF THE NUMERICAL AND FIELD EXPERIMENTS

One-dimensional elevation spectra at the measurement point obtained in the field experiment were compared with those of the numerical experiment using different parameterizations of wind effects. It is clear from Fig. 4a that the values are overestimated too much in case of using oceanic wind effects, whereas the use of the new parameterization improves the agreement between the results of the numerical and field experiments.

The comparison of integral characteristics of the spectra (significant wave heights and weighted mean period of the spectrum) was carried out for all experiments. In Fig. 4b, the black dash line is a bisectrix of the angle corresponding to the equality of the field experiment characteristics. We demonstrate data computed using the oceanic wind effects from WAM 3 and using the modified parameterization of WAM 3 with the new parameterization of C_D.

At using the oceanic model, the systematic overestimation of significant wave height is observed as well as the underestimation of weighted mean wave period. The standard deviation of the computed values of H_s for WAM 3 is 52%. The use of the new parameterization of C_D reduces the standard deviation for WAM 3 from 52 to 39%. This is an expected result because in the numerical experiment the rate of wind-induced wave growth with the proposed parameterization of C_D is specified more accurately, i.e., the amount of energy coming to the system is simulated more accurately.

However, it is clear from Fig. 4d that the prediction of weighted mean wave periods has a significant error and the correction in the specifying of the rate of wind-induced wave growth did not result in considerable changes. Perhaps, this is associated with the fact that the WAVEWATCH III model is adapted to marine conditions. This is manifested not only in the wind effect function but also in the features of parametric accounting of nonlinearity which causes the spectral redistribution of received energy. The model is intended to describe waves typical of marine and oceanic conditions that have a smaller steepness ratio as compared with the waves in a medium-size inland reservoir. Proportionality coefficients in the DIA scheme [15, 16] are adapted to marine conditions. To describe steeper waves in a medium-size inland reservoir, other adjustment parameters can be required. These parameters should correspond to the situation with more significant nonlinearity that will quicken the frequency shift towards the low-frequency range. Hence, weighted mean wave periods should also be smaller. Probably, such adaption of the scheme of nonlinearity will not affect the quality of prediction of the value of H_s characterizing the amount of energy coming to the system and will increase the accuracy of prediction of weighted mean wave periods. It is planned to test this hypothesis in future numerical experiments.

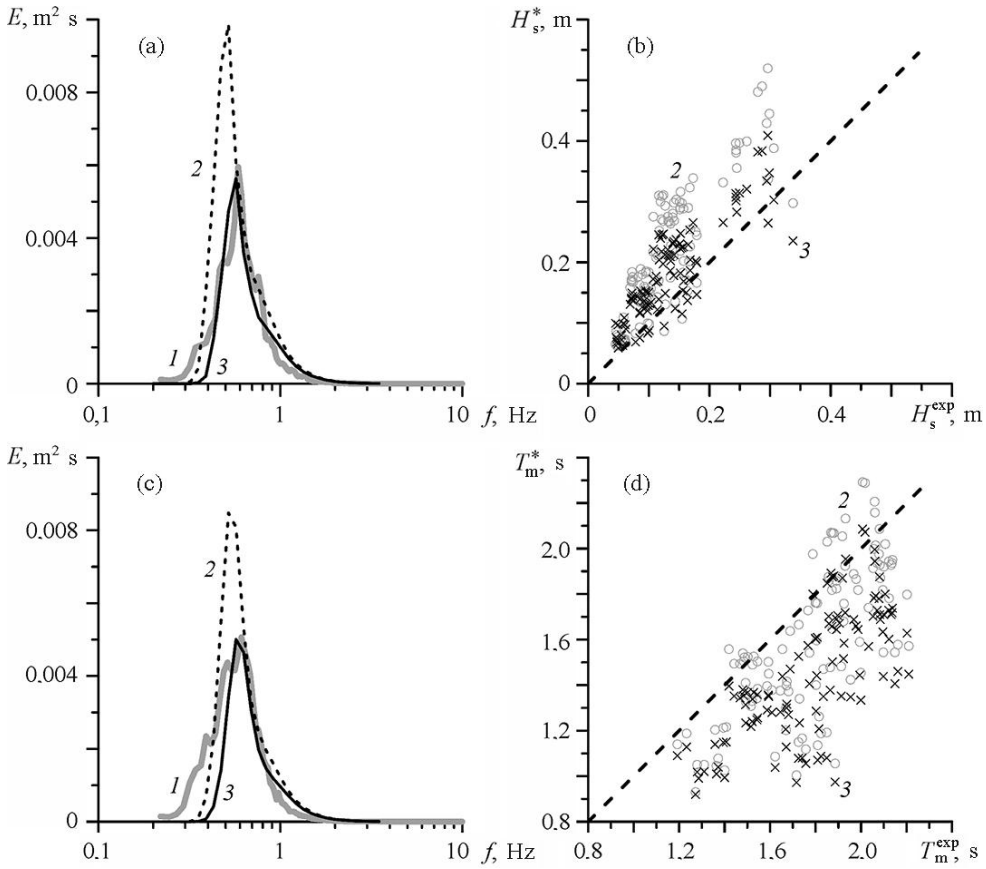

Fig. 4. The comparison of (a, c) one-dimensional overestimation spectra and integral characteristics of the spectra ((b) significant wave height H_s and (d) weighted mean wave period T_m). (*1*) Experimental values; (*2*) using the oceanic WAM 3 parameterization; (*3*) using the modified WAM 3 parameterization. H_s^* and T_m^* are the WAM 3 model data; H_s^{exp} and T_m^{exp} are experimental data.

7. CONCLUSIONS

The possibility is considered of the WAVEWATCH III model adaptation to a medium-size inland reservoir by an example of the Gorky Reservoir which was specified in the model using the NOAA GLOBE real topographic grid. To carry out the computations, the original values of model parameters were changed according to the data of field experiments in the reservoir. In particular, the minimum significant wave height was changed, the frequency range is from 0.2 to 4 Hz. The waves developed under the influence of homogeneous non-stationary wind (specified as a result of the data of the field experiment) were computed using both parameterizations of wind effects adapted to the open ocean conditions and parameterizations with the modified specification of $C_D(U_{10})$ which was obtained from field experiments. The data of field experiments in the Gorky Reservoir demonstrated that the value of the aerodynamic drag coefficient of the surface C_D in the area of moderate and strong wind is by about 50% smaller than the values typical of oceanic conditions. The results of the numerical experiment were compared with the results of the field experiment in the Gorky Reservoir. The use of the original parameterization demonstrated the considerable overestimation of the computed data on H_s as compared with the experimental data. The authors explained this by the considerable overestimation of turbulent wind stress (values of wind friction velocity u_*) and, hence, of wind effects. The use of the new parameterization of $C_D(U_{10})$ obtained from the measurement data lead to decrease in the values of u_* and, consequently, in the rate of wind-induced wave growth that improved the consistency in H_s data between the field experiment and numerical modeling. The comparison of the results of computation in the framework of original oceanic models of wind effects also demonstrated the overestimated values of weighted mean wave period T_m. At the same time, the variations of wind effects did not affect considerably agreement in the values of T_m between the results of numerical simulation and the field experiment. This is probably associated with the fact that the scheme of nonlinearity

is also adapted to marine and oceanic conditions. In the future it is necessary to adapt the parameters of DIA nonlinearity scheme to the conditions of a medium-size inland reservoir.

Besides, the use of deep water approximation for the computations can be a possible source of differences. The accounting of the real bathymetry of the Gorky Reservoir as well as the use of shallow-water-related parameterizations in WAVEWATCH III or the nesting of the SWAN model for the coastal zone can essentially improve the results.

One more source of the possible errors of the numerical experiment should also be noted. Due to the absence of sufficient experimental data, wind speed was assumed to be uniform over the whole water area of the reservoir taking into account the temporal variability specified as a result of the experiments. In reality the non-uniform distribution of wind speed and wind direction can be expected because such factors as the prolate shape of the reservoir and high shores may result in the considerable spatial variability with the scales of about or below 1 km. It is also impossible to specify wind speed from the reanalysis data due to the too low spatial resolution (2.5). The accounting of high spatial variability is a complex problem, for its solution it is planned to use high- and very-high-resolution atmospheric models (for example, WRF (Weather Research and Forecasting) with the LES (Large Eddy Simulation) block.)

ACKNOWLEDGMENTS

The research was supported by the Government of the Russian Federation (grant 11.G34.31.0048), by the grant of the President of the Russian Federation for young scientists (MK-3550.2014.5), and by the Russian Foundation for Basic Research (grants 14-05-91767, 14-05-31343, 15-35-20953, and 15-45-02580). The field experiments were supported by the Russian Scientific Foundation (grant 15-17-20009). The numerical modeling was partially supported by the Russian Scientific Foundation (grant 14-17-00667).

REFERENCES

1. G. S. Golitsyn, “The Energy Cycle of Wind Waves on the Sea Surface,” Izv. Akad. Nauk, Fiz. Atmos. Okeana, No. 1, **46** (2010) [Izv., Atmos. Oceanic Phys., No. 1, **46** (2010)].
2. S. A. Poddubnyi and E. V. Sukhova, *Modeling the Effects of Hydrodynamic and Anthropogenic Factors on the Distribution of Hydrobionts in Reservoirs. User’s Manual* (Rybinskii Dom Pechati, Rybinsk, 2002) [in Russian].
3. O. G. Setton, *Micrometeorology* (Gidrometeoizdat, Leningrad, 1958) [Transl. from Engl.]
4. E. N. Sutyrina, “Determination of Wave Characteristics in the Bratsk Reservoir,” Izvestiya Irkutskogo Gosudarstvennogo Universiteta, No. 2, **4** (2011) [in Russian].
5. G. M. Alves Jose-Henrique, A. Chawla, H. L. Tolman, et al., “The Great Lakes Wave Model at NOAA/NCEP: Challenges and Future Developments,” in *12th International Workshop on Wave Hindcasting and Forecasting, Kohala Coast, Hawaii, HI* (2011).
6. G. M. Alves Jose-Henrique, A. Chawla, H. L. Tolman, et al., “The Operational Implementation of a Great Lakes Wave Forecasting System at NOAA/NCEP,” Wea. Forecasting, **29** (2014).
7. S. S. Atakturk and K. B. Katsaros, “Wind Stress and Surface Waves Observed on Lake Washington,” J. Phys. Oceanogr., **29** (1999).
8. A. V. Babanin and V. K. Makin, “Effects of Wind Trend and Gustiness on the Sea Drag: Lake George Study,” J. Geophys. Res., **113** (2008).
9. S. E. Belcher and J. C. R. Hunt, “Turbulent Shear Flow over Slowly Moving Waves,” J. Fluid Mech., **251** (1993).
10. B. T. Brooke, “Shearing Flow over a Wavy Boundary,” J. Fluid Mech., **11** (1959).
11. M. A. Donelan, W. M. Drennan, and A. K. Magnusson, “Nonstationary Analysis of the Directional Properties of Propagating Waves,” J. Phys. Oceanogr., No. 9, **26** (1996).
12. C. W. Fairall, E. F. Bradley, J. E. Hare, et al., “Bulk Parameterization of Air–Sea Fluxes: Updates and Verification for the COARE Algorithm,” J. Climate, **16** (2003).
13. C. W. Fairall and S. E. Larsen, “Inertial-dissipation Methods and Turbulent Fluxes at the Air–Ocean Interface,” Boundary-Layer Meteorol., **34** (1986).
14. H. Gunter, S. Hasselmann, and P. A. E. M. Janssen, *The WAM Model Cycle 4. Technical Report No. 4. DKRZ WAM4 Model Documentation* (Hamburg, 1992).
15. S. Hasselmann and K. Hasselmann, “Computations and Parameterizations of the Nonlinear Energy Transfer in a Gravity-wave Spectrum. Part I: A New Method for Efficient Computations of the Exact Nonlinear Transfer Integral,” J. Phys. Oceanogr., **15** (1985).
16. S. Hasselmann, K. Hasselmann, J. H. Allender, and T. P. Barnett, “Computations and Parameterizations of the Nonlinear Energy Transfer in a Gravity-wave Spectrum. Part II: Parameterizations of Nonlinear Energy Transfer for Application in Wave Models,” J. Phys. Oceanogr., **15** (1985).

17. T. J. Hesser, M. A. Cialone, and M. E. Anderson, *Lake St. Clair: Storm Wave and Water Level Modeling* (The US Army Research and Development Center (ERDC), 2013).
18. http://polar.ncep.noaa.gov/waves/viewer.shtml?-glw-latest-hs-grl.
19. G. L. Komen, S. Hasselmann, and K. Hasselmann, "On the Existence of a Fully Developed Wind-sea Spectrum," J. Phys. Oceanogr., No. 9, **14** (1984).
20. L. J. Lopatoukhin, A. V. Boukhanovsky, E. S. Chernyshova, and S. V. Ivanov, "Hindcasting of Wind and Wave Climate of Seas around Russia," in *Proceedings of the 8th International Workshop on Waves Hindcasting and Forecasting. North Shore, Oahu, Hawaii, November 14–19, 2004*.
21. J. W. Miles, "On the Generation of Surface Waves by Shear Flows," J. Fluid Mech., **3** (1957).
22. M. Newton-Matza, *Disasters and Tragic Events: An Encyclopedia of Catastrophes in American History* (California, Santa Barbara, 2014).
23. R. L. Snyder, F. W. Dobson, J. A. Elliot, and R. B. Long, "Array Measurements of Atmospheric Pressure Fluctuations above Surface Gravity Waves," J. Fluid Mech., **102** (1981).
24. *SWAN Team. SWAN—User Manual* (Delft University of Technology, Environmental Fluid Mechanics Section, 2006).
25. H. L. Tolman and WAVEWATCH III Development Group, *User Manual and System Documentation of WAVEWATCH III Version 4.18* (Environmental Modeling Center, Marine Modeling and Analysis Branch, 2014).
26. Yu. I. Troitskaya, D. A. Sergeev, A. A. Kandaurov, et al., "Laboratory and Theoretical Modeling of Air–Sea Momentum Transfer under Severe Wind Conditions," J. Geophys. Res., **117** (2012).
27. R. O. Weber, "Remarks on the Definition and Estimation of Friction Velocity," Boundary-Layer Meteorol., **93** (1999).
28. J. Wu, "Wind-stress Coefficients over Sea Surface from Breeze to Hurricane," J. Geophys. Res., **87** (1982).
29. V. E. Zakharov, "On the Domination of Nonlinear Wave Interaction in the Energy Balance of Wind-driven Sea," in *Proceedings of 11th Wave Workshop, Halifax, Canada* (2009).